

PFC/JA-92-34

Numerical Study of Relativistic Magnetrons

H.W. Chen, C. Chen

December, 1992

Plasma Fusion Center
Massachusetts Institute of Technology
Cambridge, MA 02139 USA

Submitted for publication in Journal of Applied Physics. This work was supported in part by SDIO/IST under the management of Harry Diamond Laboratories, the Department of Energy, High Energy Physics Division, the Office of Naval Research, and the Naval Surface Warfare Center.

NUMERICAL STUDY OF RELATIVISTIC MAGNETRONS

Hei Wai Chan and Chiping Chen
Plasma Fusion Center
Massachusetts Institute of Technology
Cambridge, Massachusetts 02139
and
Ronald C. Davidson
Princeton Plasma Physics Laboratory
Princeton University
Princeton, New Jersey 08543

ABSTRACT

The relativistic multiresonator magnetron is analyzed in full cylindrical geometry, using the two-dimensional particle-in-cell simulation code MAGIC. Detailed comparisons are made between the simulation results and the classic experiments by A. Palevsky and G. Bekefi for the relativistic A6 magnetron configuration [Phys. Fluids **22**, 986 (1979)]. The computer simulations show the same dependence of microwave power on axial magnetic field as measured in the experiment. It is found that the electron flow in the preoscillation regime differs substantially from ideal Brillouin flow, and that the nonlinear regime is characterized by large-amplitude spoke formation. By analyzing a class of relativistic magnetrons for a wide range of operating voltage and axial magnetic field, it is found that the optimal microwave power exhibits an approximately cubic dependence on the applied diode voltage. Moreover, the simulations indicate that relativistic magnetrons with small aspect ratio oscillate predominantly in the π -mode, whereas magnetrons with large aspect ratio can oscillate in various modes which depend upon the system parameters. Finally, it is shown that a finite power-supply impedance can modify strongly the resonance condition, thereby significantly degrading the magnetron performance.

PACS numbers: 41.60.Cr, 41.75.Ht, 52.75.Pv, 52.25.Wz

I. INTRODUCTION

In conventional magnetrons [1],[2], voltages of a few hundred volts to tens of kilovolts are applied between an anode and a heated, thermionic cathode. Power levels from tens of watts to hundreds of kilowatts can be achieved in the decimeter and centimeter wavelength range with conversion efficiencies as high as 80%. While research on conventional magnetrons has a long history, the resurgence of interest in magnetrons has been triggered, in large part, by the pioneering work of Bekefi, Orzechowski, and Palevsky [3]-[5]. Since the classic experiments on the so-called A6 magnetron [5], which produced an unprecedented rf output power of 900 MW, the A6 magnetron configuration has become the prototype for the next generation of relativistic magnetrons [6]-[10]. In a relativistic magnetron, a field-emission diode is pulsed in the several hundred kilovolt to megavolt range in order to generate microwaves at gigawatt power levels. Intense experimental efforts in the United States and the former Soviet Union have led to the development of more powerful relativistic magnetrons in a variety of design configurations [11]-[17]. In recent years, the phenomenon of phase locking in relativistic magnetrons has been the subject of active experimental [18]-[20] and theoretical [21],[22] research.

Although magnetrons are widely used as microwave sources, a fundamental understanding of the underlying interaction physics is still being developed [7],[9], particularly in the nonlinear regime. Much of the theoretical challenge in describing multiresonator magnetron operation arises from the fact that the electrons emitted from the cathode interact in a highly nonlinear way with the electromagnetic waves in the anode-cathode gap. This is manifest through strong azimuthal bunching of the electrons and the formation of large-amplitude “spokes” in the circulating electron density. In this regard, computer simulation studies provide a particularly valuable approach to analyze the interaction physics and nonlinear electrodynamics in magnetrons.

In this paper, we report the results of a comprehensive simulation study of relativis-

tic multiresonator magnetrons in *full* cylindrical geometry, using the two-dimensional particle-in-cell (PIC) simulation code MAGIC [23]. The code includes cylindrical, relativistic, and electromagnetic effects in a fully self-consistent manner. Unlike past numerical studies [24]-[28] of relativistic magnetrons, we use an improved simulation model that allows us to examine a variety of effects in relativistic magnetrons. In particular, our investigations [29],[30] have focused on the following: (i) the characteristics of relativistic magnetrons, such as output rf power and electron flow properties; (ii) the scaling and parametric dependence of microwave emission on fundamental system parameters; and (iii) the effects of finite power-supply impedance. Preliminary results of these investigations have been published elsewhere [29].

The present work shows that many characteristics observed in the experiments on the relativistic A6 magnetron configuration can be reproduced semi-quantitatively in two-dimensional particle-in-cell computer simulations. Moreover, the present simulation studies reveal that relativistic magnetrons have the following important properties. First, in the preoscillation regime, the electron flow differs substantially from ideal Brillouin flow. Second, the microwave power from a relativistic magnetron exhibits an approximately cubic dependence on the applied diode voltage. Finally, by comparison with an ideal power supply with negligibly small internal impedance, it is shown that finite impedance of the power supply can strongly modify the resonance condition and degrade significantly the magnetron performance.

After describing briefly the numerical model (Sec. II), we discuss the results of an extensive simulation study of the A6 magnetron configuration, and compare the simulation results with experimental measurements (Sec. III). In Sec. IV, we examine the output power of a class of relativistic magnetrons for a wide range of operating voltage and axial magnetic field, and show that there is a power-law scaling relation between the optimal microwave power and the applied diode voltage. In Sec. V, we address the question of

how geometric parameters, particularly the diode aspect ratio, affect the process of mode selection in a relativistic magnetron. It is also shown that the finite impedance of the power supply can have a strong influence on relativistic magnetron performance.

II. NUMERICAL MODEL

In the simulations, cylindrical, relativistic, and electromagnetic effects are included in a fully self-consistent manner. The two-dimensional Maxwell equations and three-dimensional relativistic particle orbit equations are integrated numerically for about 4×10^4 time steps, using more than 3×10^4 macroparticles and a nonuniform, two-dimensional grid consisting of approximately 3×10^3 cells. A radially nonuniform grid is used to resolve small-scale variations in the particle velocities and positions and field quantities, particularly in the interaction region ($a \leq r \leq b$). The cross section of the A6 magnetron configuration is illustrated in Fig. 1, where the applied axial magnetic field ($B_f \vec{e}_z$) points out of the page and provides magnetic insulation of the electron flow. The simulations are performed using MAGIC [23], a two-dimensional particle-in-cell (PIC) code developed by B. Goplen, *et al.*

In the simulations, the anode and the cathode are taken to be perfect conductors, and the rf power is extracted through an output window placed in an open resonator along the dashed line in Fig. 1. At the window, the boundary conditions are such that most of the electromagnetic wave energy is absorbed, whereas a negligibly small fraction of the wave energy is reflected back into the cavity. Such a window yields an effective quality factor of $Q \approx 100$ for the A6 magnetron oscillator. The rf power delivered to the window (i.e., the rf power output) is given by the net flow of electromagnetic energy expressed as an area-integral of the Poynting flux through the window surface.

The electrons are emitted from the cathode through a space-charge-limited field emission process in which the instantaneous electric field normal to the cathode surface van-

ishes. On the other hand, electrons are absorbed by the anode or the cathode whenever they strike the anode or cathode surface.

An important aspect of the simulation model concerns the application of a high-voltage pulse from an external power supply to the magnetron diode. Because the voltage pulse rises slowly compared with the electron cyclotron period and the rf oscillation period, the magnetic field induced by the changing voltage pulse is neglected, and a quasi-static model is used to describe the high-voltage pulse. In this model, the diode voltage is given by

$$V_D(t) = \frac{Z(t)V_0(t)}{Z_0 + Z(t)}, \quad (1)$$

where $V_0(t)$ is the voltage pulse provided by the power supply, $Z_0 = \text{const}$ is the internal impedance of the power supply, and $Z(t)$ is the magnetron impedance. The magnetron impedance $Z(t)$ and the diode voltage $V_D(t)$ are determined self-consistently in the simulations. For an ideal power supply with $Z_0 = 0$, the diode voltage is given simply by $V_D(t) = V_0(t)$. In the simulations, the voltage pulse $V_0(t)$ is assumed to have the form

$$V_0(t) = \begin{cases} 0, & t < 0, \\ (t/t_0)V_m, & 0 \leq t < t_0, \\ V_m, & t \geq t_0, \end{cases} \quad (2)$$

where t_0 and V_m are the rise time and maximum value of the voltage pulse, respectively. Typically, the rise time assumed in the simulations is $t_0 = 4.0$ ns, corresponding to the experimental value [5]. Although the applied voltage pulse is described approximately by Eq. (2), it should be emphasized that all extraordinary-mode rf excitations, $\delta\vec{B}(r, \theta, t) = \delta B_z(r, \theta, t)\hat{e}_z$ and $\delta\vec{E}(r, \theta, t) = \delta E_r(r, \theta, t)\hat{e}_r + \delta E_\theta(r, \theta, t)\hat{e}_\theta$, are treated fully electromagnetically in the simulations.

III. SIMULATION OF THE A6 MAGNETRON

The A6 magnetron configuration [5], which demonstrated in the late 1970s microwave emission at unprecedented high power levels, has become the prototype for relativistic

magnetron design [6]. We have conducted an extensive simulation study of this configuration, and because the A6 configuration was well-diagnosed in the experiments by Palevsky and Bekefi [5], we are able to make detailed comparisons between the simulations and the experimental results. Selected results reported earlier in [29] are reviewed in Secs. III.A and III.B.

A. Microwave Emission

Figure 2 shows the time history of the integrated rf field $V_\theta(t) = \int_{p_1}^{p_2} d\theta r_l \delta E_\theta(r_l, \theta, t)$, and the magnitude of the Fourier transform of $V_\theta(t)$, denoted by $|\hat{V}_\theta(f)|$, for the following choice of system parameters: $B_f = 7.2$ kG, $V_m = 350$ kV, $t_0 = 4.0$ ns, and $Z_0 = 0$. The integration path corresponds to the dotted line in Fig. 1 from p_1 to p_2 at $r = r_l = 3.7$ cm. In Fig. 2(a), the nonlinear saturation of the magnetron oscillations occurs at $t \simeq 10$ ns, where the ratio of saturated wave amplitude V_{θ_s} and the applied diode voltage $V_D = V_m$ is $V_{\theta_s}/V_D \simeq 0.85$. In Fig. 2(b), the two distinct peaks at the frequencies $f = 2.0$ GHz and $f = 4.0$ GHz correspond to the π -mode ($l = 3$) and 2π -mode ($l = 6$) oscillations, respectively. For the A6 magnetron, by a coincidence of design, the frequency of the 2π -mode is twice the frequency of the π -mode. By examining the relative phase of the adjacent resonators, the peak at $f = 4.0$ GHz is identified as the 2π -mode rather than the second harmonic of the π -mode. The 2π -mode oscillation frequency $f = 4.0$ GHz is 14% lower than the frequency $f = 4.55$ GHz observed in the experiment [5]. This is likely due to the neglect of finite-axial-length effects in the simulations which assume $\partial/\partial z = 0$. Indeed, if the axial mode number $n = 1$ is assumed, then a simple estimate of the (corrected) 2π -mode oscillation frequency is $f_1 = f[1 + (c/2Lf)^2]^{1/2}$. Substituting $f = 4.0$ GHz and the diode length $L = 7.2$ cm gives $f_1 = 4.5$ GHz.

By evaluating the area-integral of the outward Poynting flux $(c/4\pi)\delta E_\theta \delta B_z$ over the window surface at $r = d = 4.11$ cm in Fig. 1, the rf power output is calculated for various values of the applied magnetic field B_f . The magnetic field dependence of the normalized

rf power is shown in Fig. 3, where the solid circles correspond to the experimental values and the solid triangles are obtained from the simulations with $V_m = 350$ kV, $t_0 = 4.0$ ns, and $Z_0 = 0$. In Fig. 3, the normalization is chosen such that the maximum values of the rf power in the simulations and in the experiments are equal to unity. The actual value of the maximum rf power output per unit axial length in the simulations is 4.3 GW per meter length of the diode. For the A6 magnetron, which has a *geometric* axial length $L = 7.2$ cm, this corresponds to a maximum rf power of $P = 0.3$ GW, which is somewhat less than the maximum rf power $P = 0.45$ GW measured in the experiment [5]. The values of power quoted here are rms values. Apart from a constant scale factor between the rf powers obtained in the experiments and in the simulations, it is evident from Fig. 3 that the dependence of the rf power on applied magnetic field obtained in the simulations is in very good agreement with the experimental results. The difference in scale factor is most likely due to the fact that the *effective* axial length of the A6 magnetron is greater than its geometric axial length [6].

Three remarks are in order concerning the simulation results shown in Fig. 3. First, we are unable to obtain from the simulations the rf power for $B_f < 6.0$ kG. As the axial magnetic field B_f is decreased from 6.0 kG, the diode current becomes increasingly large, as will be shown later in Fig. 6. This results in a rapid decrease in the diode impedance Z . For example, the impedance of the A6 magnetron diode at $B_f = 5.5$ kG is estimated to be $Z_0 = 3 \Omega$ from the simulations, which is comparable to the internal impedance $Z_0 = 4 \Omega$ of the power supply in the experiments [5]. Therefore, the approximation of an ideal power supply (with $Z_0 = 0$) in the simulations is no longer valid for $B_f < 6.0$ kG.

Second, the simulation results show, in good agreement with experiment, that the operating range of the magnetron is determined approximately by the Hull cutoff condition [8] and the Buneman-Hartree threshold condition [8], which predict that strong magnetron oscillations occur in the range of axial magnetic field from $B_f = 5.1$ kG to

$B_f = 8.5$ kG for $V_D = 350$ kV. Note that both conditions are derived on the basis of the Brillouin flow model. The fact that there is microwave emission outside the range predicted by these conditions suggests that kinetic effects [31], which are not included in the Brillouin flow model, may play an important role in determining the exact range for relativistic magnetron oscillations.

Finally, it should be pointed out that two-dimensional simulations are most likely to be valid if the end effects are negligibly small. Because the axial length of the A6 magnetron configuration [5], $L = 7.2$ cm, is long compared with the width of the interaction region, $b - a = 0.53$ cm, the basic interaction physics of the A6 magnetron should be modeled well by the present two-dimensional simulations. Indeed, many characteristics of the A6 magnetron observed in the experiments are reproduced semi-quantitatively in the two-dimensional simulations, as shown in Figs. 2 and 3. For relativistic magnetrons with a disc-like washer cathode, three-dimensional effects are expected to have a strong influence, as indicated in the recent work by Stark, *et al.* [32].

B. Electron Flow Properties

Electron flow properties in the relativistic A6 magnetron have also been examined numerically. Figure 4 shows radial plots of the azimuthally-averaged charge density $e\langle n_e \rangle(r, t) = (2\pi)^{-1} \int_0^{2\pi} en_e(r, \theta, t) d\theta$ at several instants of time for the same values of system parameters as in Fig. 2. In Fig. 4, the outer radius of the electron layer [$r = r_b(t)$], designated by the arrows, is calculated from a simple Brillouin-flow model for $B_f = 7.2$ kG and diode voltages $V_D(t) = 0.5 V_m, 0.75 V_m,$ and $1.0 V_m$, corresponding to $t = 2.0, 3.0,$ and 4.0 ns. It is clear from Fig. 4 that a substantial fraction of the electrons occupy the region between $r = r_b$ and the anode ($r = b$). The long tail in the electron density profile indicates that the electron flow is significantly different from the ideal Brillouin flow model [8]. For the A6 magnetron operating at $V_m \simeq 350$ kV, cylindrical and relativistic effects are relatively small. [For example, at $t = t_0 = 4.0$ ns, the layer aspect ratio is

$a/(r_b - a) \approx 15$, and the relativistic mass factor at $r = r_b$ is $\gamma_e^0(r_b) \approx 1.15$.] We define the local self-field parameter [8]

$$s_e(r) = \frac{\omega_{pe}^2(r)/\gamma_e^0(r)}{\omega_{ce}^2(r)/\gamma_e^{02}(r)}, \quad (3)$$

where $\omega_{pe}^2(r)/\gamma_e^0(r)$ is the (local) relativistic plasma frequency-squared and $\omega_{ce}(r)/\gamma_e^0(r)$ is the (local) relativistic cyclotron frequency. Note from Eq. (3) that $s_e = 1$ under ideal Brillouin flow conditions (in the planar approximation) [8]. In the simulations, however, it is found that the self-field parameter $s_e(r)$ decreases considerably as r increases from $r = a$ to $r = r_b$ and beyond. Indeed, for the curve corresponding to $t = t_0 = 4.0$ ns in Fig. 4, the self-field parameter decreases from $s_e(r = a) \simeq 1.0$ at the cathode to $s_e(r = r_b) \simeq 0.5$ at $r = r_b$.

Although the azimuthal bunching of the electrons is relatively small for $t \leq 4$ ns, as seen in Fig. 5(a), by $t \approx 6$ ns the system begins to enter a nonlinear regime characterized by the formation of a large-amplitude, coherent, rotating spoke structure. Highly developed spokes are evident in Fig. 5(b), which shows density-contour plots at $t = 8$ ns. The appearance of three spokes is a result of the interference between the π -mode and the 2π -mode oscillations. As the system evolves, the spokes rotate azimuthally in synchronism with the rf waves for many circulation periods around the magnetron, sustaining high-current flow from the cathode to the anode. By saturation ($t \approx 10$ ns), the time-averaged (dc) diode current per unit axial length is $I_D = 100$ kA/m, and the oscillating (ac) diode current is comparable to I_D . The amplitude of the integrated rf field profile $\int_a^b dr \delta E_r(r, \theta, t)$ is also comparable to the diode voltage $V_D = V_m = 350$ kV.

C. Beam Loading

The presence of the intense nonneutral electron flow can alter the properties of a relativistic magnetron oscillator, such as the output frequency and the quality factor of an oscillating mode. This phenomenon is known as *beam loading*. A measure of beam loading in a relativistic magnetron is the diode current or the characteristic electron

density. By varying the diode current, which can be accomplished by changing the axial magnetic field B_f , we have been able to examine qualitatively the effect of beam loading on the magnetron oscillation frequency.

Figure 6 shows the time-averaged diode current and the frequencies of the π -, 2π -, and $5\pi/3$ -mode oscillations as a function of the magnetic field B_f for the A6 magnetron configuration for the same choice of system parameters as in Fig. 3. As the diode current increases (by decreasing the magnetic field B_f), the emission frequencies decrease, as evident from Fig. 6. On the other hand, as the diode current decreases (by increasing the magnetic field B_f), the emission frequencies approach the values $f = 2.3, 4.55$, and 5.0 GHz, which are the same as those calculated from the vacuum dispersion relation [5] for the π -, 2π -, and $5\pi/3$ -modes, respectively. Note that only for an ideal power supply (with $Z_0 = 0$) are the results shown in Fig. 6 applicable for $B_f < 6.0$ kG.

IV. MICROWAVE POWER SCALING

The results presented in Sec. III.A show that at a given diode voltage, the dependence of rf power on the applied axial magnetic field B_f is a bell-shaped tuning curve which achieves the optimum (i.e., maximum) rf power at some value intermediate between the Hull-cutoff and the Buneman-Hartree threshold curves [8]. For a given value of axial magnetic field B_f , a similar bell-shaped tuning curve is obtained as the applied diode voltage V_m is varied. It is natural to ask how the optimal rf power of a relativistic magnetron scales with the applied diode voltage. To answer this important question, we have studied the performance of two relativistic magnetrons, namely the A6 configuration, and a modified A6 configuration known as the SM2 configuration [20], both representing a class of six-vane relativistic magnetrons. The six-vane SM2 magnetron [20] has cathode radius $a = 0.5$ cm, anode radius $b = 1.85$ cm, and vane radius $d = 3.68$ cm. The axial magnetic field is scanned to optimize the total microwave emission for applied diode

voltages in a typical operating range of 100 kV to 1 MV. In this study, we assume an ideal power supply with internal impedance $Z_0 = 0$.

Figure 7 shows plots of the maximum rf power output versus the applied diode voltage V_D for the A6 and SM2 magnetrons. Taking the least-squared fit of the simulation data, we find that the optimal total microwave power exhibits an approximately cubic dependence on the diode voltage, i.e.,

$$P \propto V_D^\alpha, \quad (4)$$

where $\alpha \cong 2.9$ and $\alpha \cong 3.1$ for the A6 and SM2 magnetron configurations, respectively, and V_D is the flat-top voltage of the applied voltage pulse. The scaling relation in Eq. (4) differs from the expected power scaling, $P \propto V_D^{5/2}$, which may be obtained from the following estimate. Let us assume that $P \propto I_D V_D$, where I_D is the dc diode current in the presence of an axial magnetic field but in the absence of rf field. Based on the analysis in [33], the dc diode current is given by $I_D \propto V_D^{3/2}$, which has the same scaling as given by the Child-Langmuir law [34],[35] in the absence of both axial magnetic field and rf field. Substituting $I_D \propto V_D^{3/2}$ into $P \propto I_D V_D$ yields $P \propto V_D^{5/2}$.

It is possible that the presence of large-amplitude rf fields may account for the higher conducting current in relativistic magnetrons, thereby yielding a larger exponent than the expected value. Investigations of this possibility require the development of a fully nonlinear, electromagnetic theory of the relativistic magnetron. Finally, it should be noted that the two-dimensional simulation model used here does not take into account the loss of axial current due to $E_r \vec{e}_r \times B_\theta \vec{e}_\theta$ drifts in magnetron operation. The electrons lost axially do not contribute towards microwave generation, and therefore reduce the overall efficiency of the relativistic magnetron [6].

V. PARAMETRIC STUDIES

A. Mode Selection

The process of mode selection in a self-oscillating relativistic magnetron has been studied qualitatively by varying the cathode and anode radii a and b , and the vane depth $d - b$. In particular, the dependence of mode excitations on the diode aspect ratio $A = a/(b - a)$ has been analyzed for a class of six-vane magnetrons with geometric parameters derived from the A6 magnetron. Simulation studies indicate that magnetrons with small aspect ratio (i.e., $A < 1$) tend to oscillate predominantly in the π -mode for a wide range of diode voltages and magnetic field values, whereas magnetrons with large aspect ratio (i.e., $A > 1$) oscillate, depending upon system parameters, in various modes such as the π -mode and the 2π -mode.

Figure 8(a) shows, for a magnetron with the small aspect ratio $A = 0.4$, that only the π -mode can be excited for magnetic field values ranging from the Hull cutoff curve to the Buneman-Hartree threshold curves, $V_{\text{BH}}(\pi)$ and $V_{\text{BH}}(2\pi)$ for the π -mode and the 2π -mode, respectively. This result supports the qualitative arguments by Palevsky and Bekefi[5] that magnetrons with a large anode-cathode gap (small-aspect-ratio) favor π -mode operation. Because the electric field excitation for the 2π -mode is mostly azimuthal near the cathode, it is plausible to argue that the 2π -mode does not interact strongly with the electrons, thereby resulting in a relatively weak azimuthal bunching and energy transfer from the electrons to the rf field. On the other hand, the radial and azimuthal components of the electric field for the π -mode are comparable in magnitude near the cathode, and the π -mode field pattern allows for a strong coupling of the electromagnetic wave with the circulating electron flow.

In a magnetron with the large aspect ratio $A = 4.7$, it is found that the π -, 2π - and $5\pi/3$ -modes can be excited, either independently, or in combination within the Hull cutoff curve and the Buneman-Hartree threshold curve $V_{\text{BH}}(\pi)$ for the π -mode, as il-

illustrated in Fig. 8(b). Because the radial and azimuthal components of the electric field for the π -mode, the 2π -mode, and the $5\pi/3$ -mode are comparable in magnitude near the cathode, a strong coupling of these modes with the circulating electron layer can be realized by increasing the magnetic field so that the electron flow is tuned successively in resonance with the π -mode, the 2π -mode, and the $5\pi/3$ -mode. This is also true for the A6 magnetron, which has the aspect ratio $A = 3.0$, as discussed in Sec. III.

B. Effects of Finite Impedance of the Power Supply

The high conducting current of a fully oscillating, relativistic magnetron can result in a significant voltage drop across the (finite) impedance of the power supply. Thus, in comparison with an ideal power supply, we expect the following effects: (i) a significant change in the resonance condition; (ii) a decrease of the diode voltage; and (iii) a degradation in magnetron performance (because of the lower diode voltage). To gain a better understanding of these effects, in the simulations we have used the impedance model described earlier in Sec. II.A, assuming that Z_0 is resistive, corresponding to a real, non-zero value.

Figure 9 shows a shift in the tuning curve for $Z_0 \neq 0$ in comparison with the tuning curve for $Z_0 = 0$. The results in Fig. 9 have been obtained from the simulations for the choice of applied voltage pulse $V_0(t)$ in Eq. (2), with $V_m = 470$ kV, $t_0 = 4.0$ ns, and $Z_0 = 14 \Omega$. In Fig. 9, it is evident for $Z_0 \neq 0$ that the 2π -mode tuning curve for maximum microwave emission is shifted closer to the Hull cutoff curve.

Figure 10 illustrates the reduction in diode voltage V_D corresponding to the case where the internal impedance is $Z_0 = 14 \Omega$ in Fig. 9. The dashed curve in Fig. 10 corresponds to the experimental measurements [5]. Because the precise value of the applied voltage V_0 in the experiments [5] is not available, a detailed comparison cannot be made between the simulation studies and the experiments in which $Z_0 = 4 \Omega$. In any case, the basic feature is well-illustrated in Fig. 10. That is, for a given voltage pulse, a finite power

supply impedance reduces the diode voltage, particularly in the vicinity of the Hull cutoff curve.

VI. CONCLUSIONS

The fundamental interaction physics and nonlinear electrodynamics in relativistic magnetrons have been analyzed using two-dimensional particle-in-cell simulations. The present analysis incorporated the full effects of cylindrical geometry with corrugated anode boundary. It was shown, for the first time, that many characteristics observed in relativistic A6 magnetron experiments can be reproduced semi-quantitatively using two-dimensional particle-in-cell computer simulations. In particular, the simulation results showed the same dependence of microwave power on magnetic field as measured in the A6 magnetron experiments [5].

It was also found that the electron flow in the preoscillation regime differs substantially from ideal Brillouin flow, and that the nonlinear regime is characterized by large-amplitude spoke formation. Moreover, the frequency of magnetron oscillations was observed to decrease as the beam loading becomes more pronounced. By analyzing a class of relativistic magnetron configurations over a wide range of operating voltage and axial magnetic field, it was shown that the optimal microwave power emission exhibits an approximately cubic dependence on applied diode voltage. The simulations indicated that magnetrons with small aspect ratio oscillate predominantly in π -mode, whereas magnetrons with large aspect ratio can oscillate in various modes which depend upon the system parameters. Finally, it was shown that finite impedance of the power supply can modify strongly magnetron tuning features, thereby significantly degrading performance.

ACKNOWLEDGMENTS

The authors wish to thank George Bekefi and Shien Chi Chen for helpful discussions,

and Bruce Goplen and Larry Ludeking of Mission Research Corporation for consultations on the MAGIC simulation code. This work was supported in part by SDIO/IST under the management of Harry Diamond Laboratories, the Department of Energy High Energy Physics Division, the Office of Naval Research, and the Naval Surface Warfare Center.

The research by one of the authors (H.W. Chan) was in partial fulfillment of the requirements for the Ph.D. degree.

References

- [1] *Microwave Magnetrons*, edited by G.B. Collins (McGraw-Hill, New York, 1948).
- [2] *Crossed-Field Microwave Devices*, edited by F. Okress (Academic Press, New York, 1961), Volumes 1 and 2.
- [3] G. Bekefi and T.J. Orzechowski, *Phys. Rev. Lett.* **37**, 379 (1976).
- [4] T. J. Orzechowski and G. Bekefi, *Phys. Fluids* **22**, 978 (1979).
- [5] A. Palevsky and G. Bekefi, *Phys. Fluids* **22**, 986 (1979).
- [6] J. Benford, in *High-Power Microwave Sources*, edited by V. L. Granatstein and I. Alexeff (Artech, Boston, MA, 1987), pp. 351-395.
- [7] Y.Y. Lau, in *High-Power Microwave Sources*, edited by V. L. Granatstein and I. Alexeff (Artech, Boston, MA, 1987), pp. 309-349.
- [8] R.C. Davidson, *Physics of Nonneutral Plasmas* (Addison-Wesley, Reading, MA, 1990), Chapter 8.
- [9] R.C. Davidson, H.W. Chan, C. Chen, and S. Lund, *Rev. Mod. Phys.* **63**, 341 (1991).

- [10] J. Benford and J. Swegle, *High Power Microwaves* (Artech, Boston, MA, 1992), Chapter 5.
- [11] N.F. Kovalev, B.D. Kolchuqin, V.E. Nechaev, M.M. Ofitserov, E.I. Soluyanov, and M.I. Fuks, *Sov. Tech. Phys. Lett.* **3**, 10 (1977).
- [12] N.F. Kovalev, E.G. Krastelev, M.I. Kuznetsov, A.M. Maine, M.M. Ofitserov, V.A. Papdichev, M.I. Fuks, and L.N. Chekanova, *Sov. Tech. Phys. Lett.* **6**, 4 (1980).
- [13] A.N. Didenko, A.S. Sulakshin, G.P. Fomenko, Yu.G. Shtein, and Yu.G. Yushkov, *Sov. Tech. Phys. Lett.* **4**, 1 (1978).
- [14] I.Z. Gleizer, A.N. Didenko, A.S. Sulakshin, G.P. Fomenko, and V.I. Tsvetkov, *Sov. Tech. Phys. Lett.* **6**, 1 (1980).
- [15] H. Sze, B. Harteneck, J. Benford, and T.S.T. Young, *IEEE Trans. Plasma Science* **PS-15**, 327 (1987).
- [16] R.A. Close, A. Palevsky, and G. Bekefi, *J. Appl. Phys.* **54**, 4147 (1983).
- [17] W.P. Ballard, S.A. Self, and F.W. Crawford, *J. Appl. Phys.* **53**, 7580 (1982).
- [18] J. Benford, H.M. Sze, W. Woo, R.R. Smith, and B. Harteneck, *Phys. Rev. Lett.* **62**, 969 (1989).
- [19] T.A. Treado, R.S. Smith, 3rd., C.S. Shaughnessy, and G.E. Thomas, *IEEE Trans. Plasma Science* **PS-18**, 594 (1990).
- [20] S.C. Chen, G. Bekefi, and R.J. Temkin, in *Intense Microwave and Particle Beams II*, edited by H.E. Brandt, *Proc. SPIE* **1407**, 67 (1991).
- [21] W. Woo, J. Benford, D. Fittinghoff, B. Harteneck, D. Price, R. Smith, and H. Sze, *J. Appl. Phys.* **65**, 861 (1989).

- [22] S.C. Chen, IEEE Trans. Plasma Science **PS-18**, 570 (1990).
- [23] B. Goplen, *et al.*, MAGIC User's Manual (MRC Report MRC/WDC-R-184, Mission Research Corporation, Newington, VA 22122, 1988).
- [24] O. Buneman, in *Crossed-Field Microwave Devices*, edited by F. Okress (Academic Press, New York, 1961), Volume 1, p. 209.
- [25] S.P. Yu, G.P. Kooyers, and O. Buneman, J. Appl. Phys. **36**, 2550 (1965).
- [26] A. Palevsky, G. Bekefi, and A.T. Drobot, J. Appl. Phys. **52**, 4938 (1981).
- [27] A. Palevsky, G. Bekefi, A. Drobot, A. Mondelli, G. Graig, K. Eppley, M. Black, M. Bollen, and R. Parker, in *High-Power Beams*, edited by H.J. Doucet and J.M. Buzzi, (Ecole Polytechnique, Palaiseau, France, 1981), p. 861.
- [28] B. Marder, J. Comput. Phys. **68**, 48 (1987).
- [29] H.W. Chan, C. Chen, and R.C. Davidson, Appl. Phys. Lett. **57**, 1271 (1990).
- [30] H.W. Chan, Ph.D. Dissertation, Massachusetts Institute of Technology (1992).
- [31] H.S. Uhm, Phys. Fluids **B4**, 740 (1992).
- [32] R.A. Stark, H.C. Chen, and H.S. Uhm, in *Intense Microwave and Particle Beams II*, edited by H.E. Brandt, Proc. SPIE **1407**, 128 (1991).
- [33] L. Brillouin, Phys. Rev. **67**, 260 (1945).
- [34] C.D. Child, Phys. Rev. **32**, 492 (1911).
- [35] I. Langmuir, Phys. Rev. **2**, 450 (1913).

FIGURE CAPTIONS

- Fig. 1 Cross section of the A6 magnetron configuration. The rf power is absorbed by an output window (dashed line) located at $r = d = 4.11$ cm in the open resonator. Here, $a = 1.58$ cm, $b = 2.11$ cm, $d = 4.11$ cm, and $\psi = 20^\circ$.
- Fig. 2 (a) Time history of the integrated rf field $V_\theta(t)$ at $r = r_l = 3.7$ cm, for $B_f = 7.2$ kG, $V_m = 350$ kV, $t_0 = 4.0$ ns, and $Z_0 = 0$. (b) The Fourier spectrum of the signal in (a).
- Fig. 3 Plots of the normalized rf power versus the applied axial magnetic field B_f .
- Fig. 4 Plots of the azimuthally averaged charge density $e\langle n_e \rangle(r, t)$ versus the radial distance r at times $t = 2.0, 3.0,$ and 4.0 ns, obtained from the simulations for the same system parameters as in Fig. 2.
- Fig. 5 Density contour plots for $n_e(r, \theta)$ obtained from the simulations at (a) $t = 3.0$ ns and (b) $t = 8.0$ ns for the same system parameters as in Fig. 2.
- Fig. 6 Plots of the time-averaged diode current (dashed curve) and the frequencies (solid curves) of the π -, 2π -, and $5\pi/3$ -mode versus the magnetic fill field B_f . Note that the diode current I_D increases rapidly as the fill field B_f decreases from 6.0 kG.
- Fig. 7 Plots of the total microwave power versus the applied diode voltage V_D for the A6 and SM2 magnetron configurations.
- Fig. 8 Mode excitations for various operating parameters corresponding to: (a) $A = 0.4$ with $a = 0.57$ cm, $b = 1.92$ cm, $d = 3.42$ cm, and $\psi = 20^\circ$; and (b) $A = 4.7$ with $a = 1.74$ cm, $b = 2.11$ cm, $d = 4.11$ cm, and $\psi = 20^\circ$.
- Fig. 9 Plots of the microwave power versus the magnetic fill field B_f for the A6 magnetron. The squares correspond to a non-ideal case with $Z_0 = 14 \Omega$ and $V_m = 470$ kV, whereas the triangles correspond to an ideal case with $Z_0 = 0$ and $V_m = 350$ kV.

Fig. 10 Plots of the diode voltage V_D versus the magnetic fill field B_f for the A6 magnetron. The squares correspond to a non-ideal case with $Z_0 = 14 \Omega$ and $V_m = 470$ kV, whereas the triangles correspond to an ideal case with $Z_0 = 0$ and $V_m = 350$ kV.

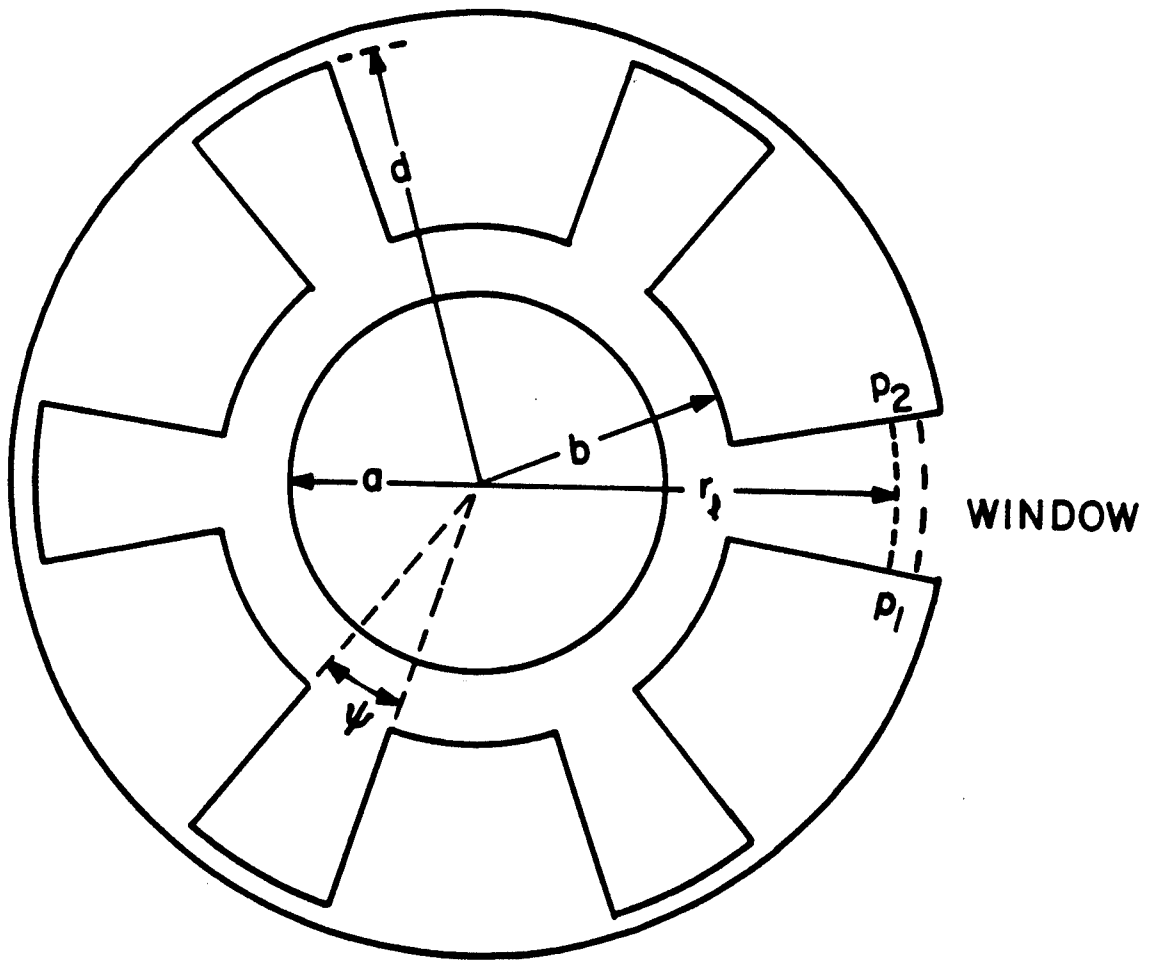


Fig. 1

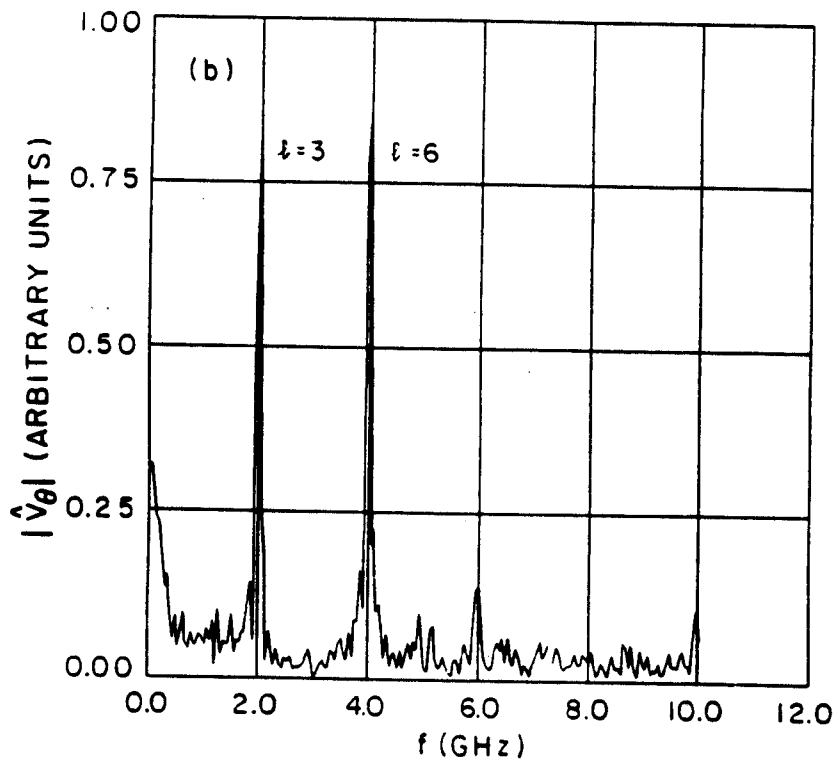
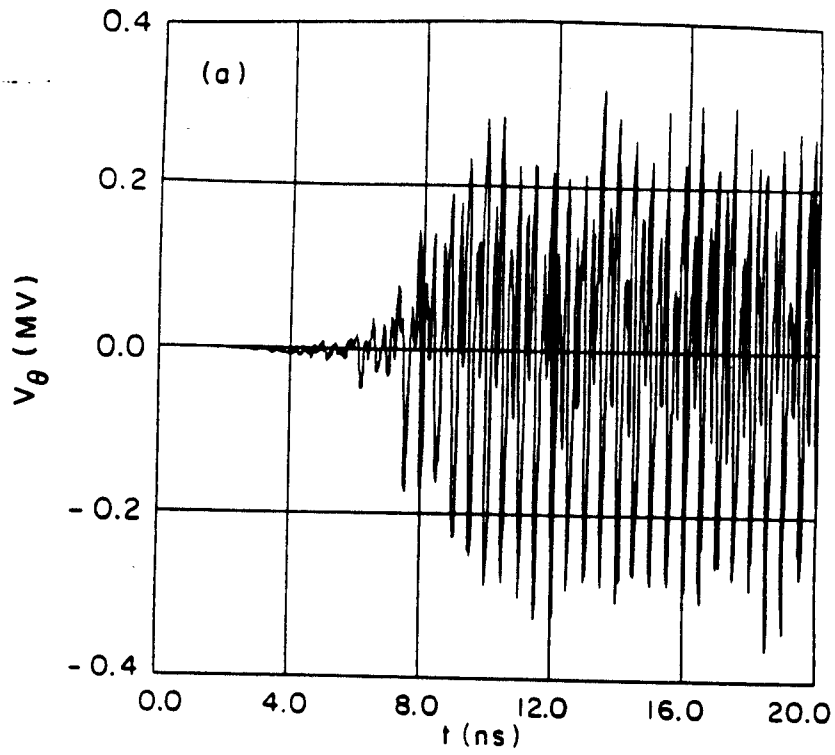


Fig. 2

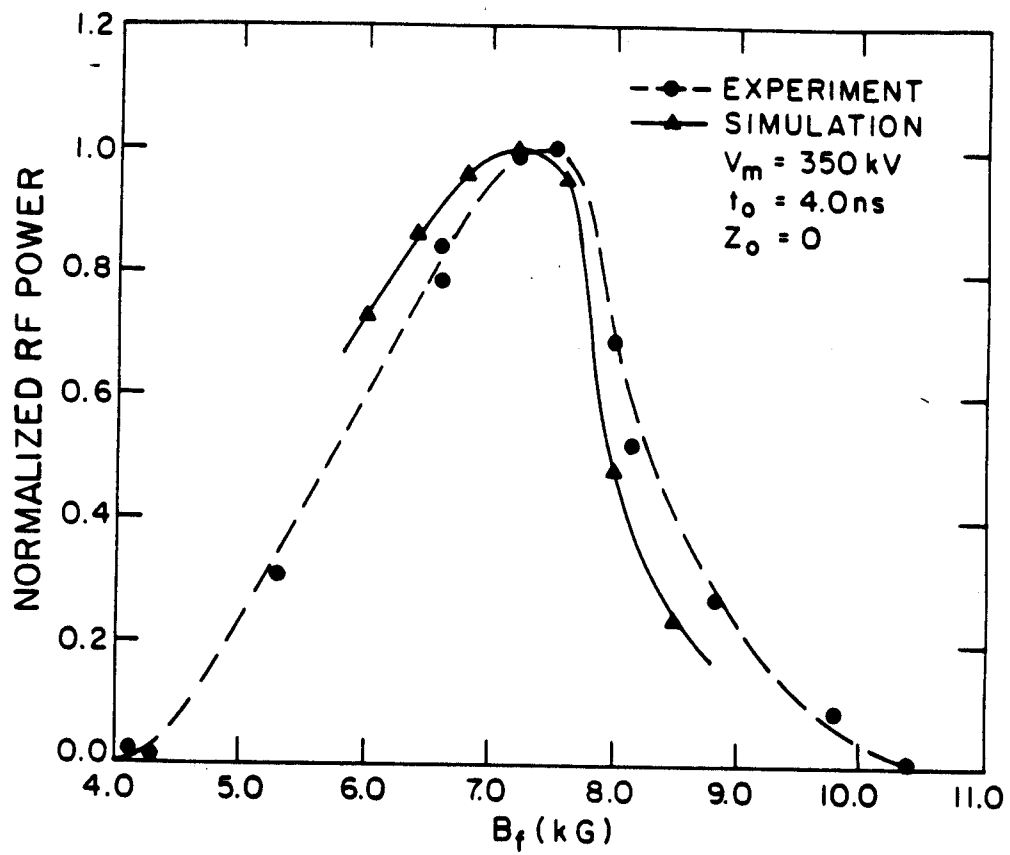


Fig. 3

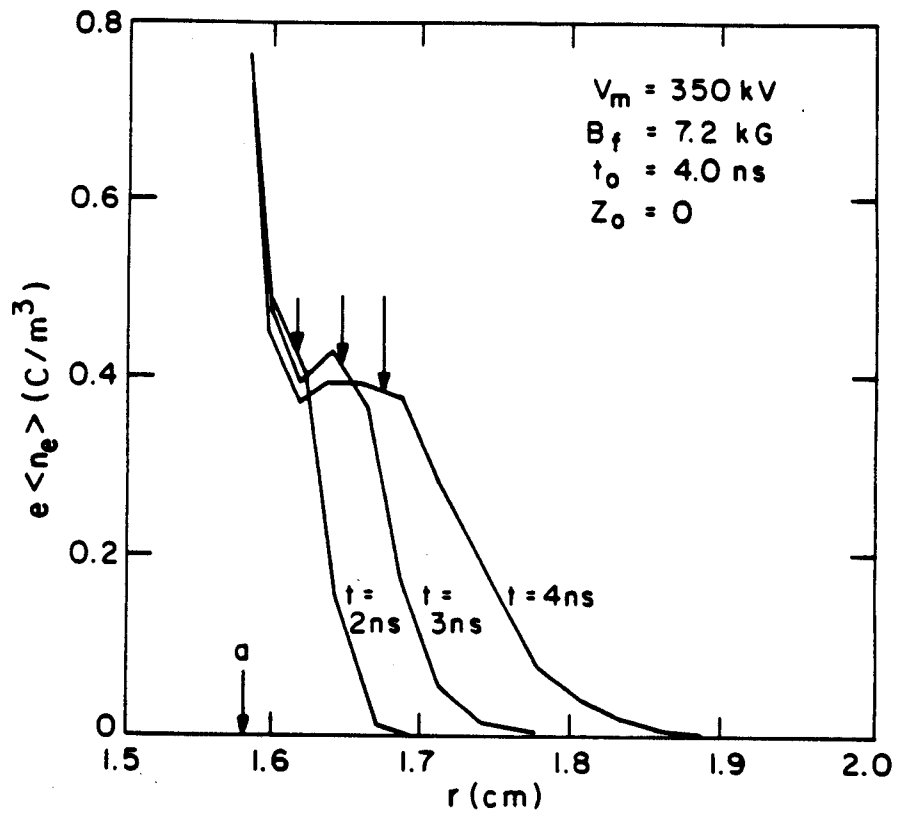


Fig. 4

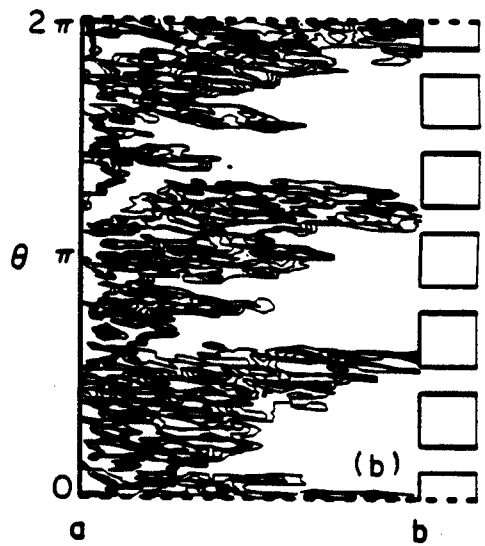
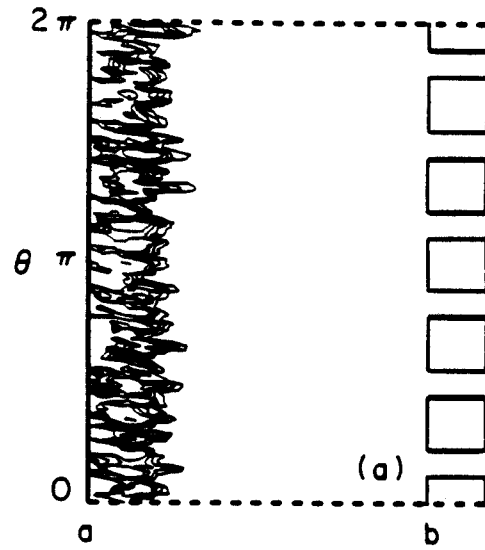


Fig. 5

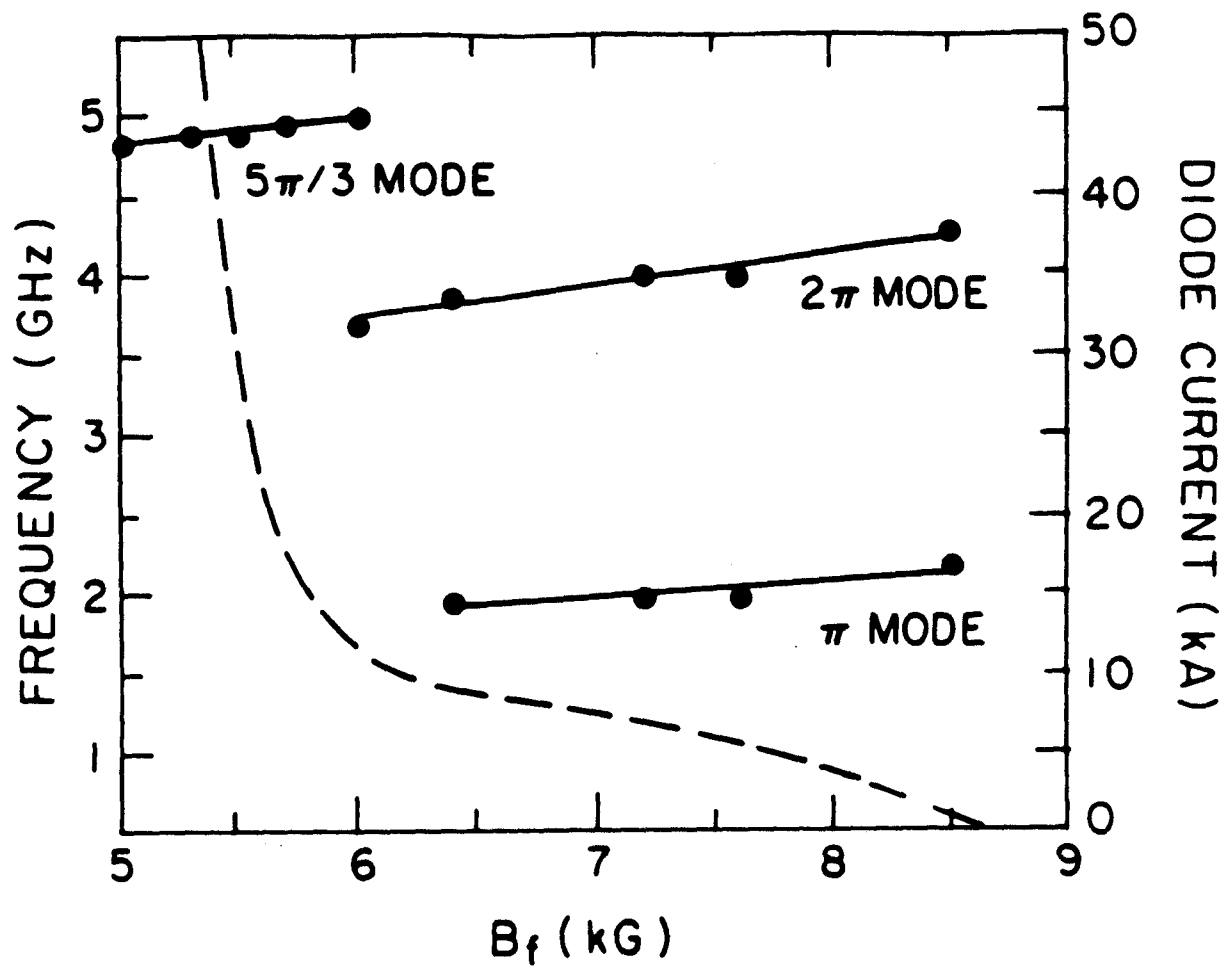


Fig. 6

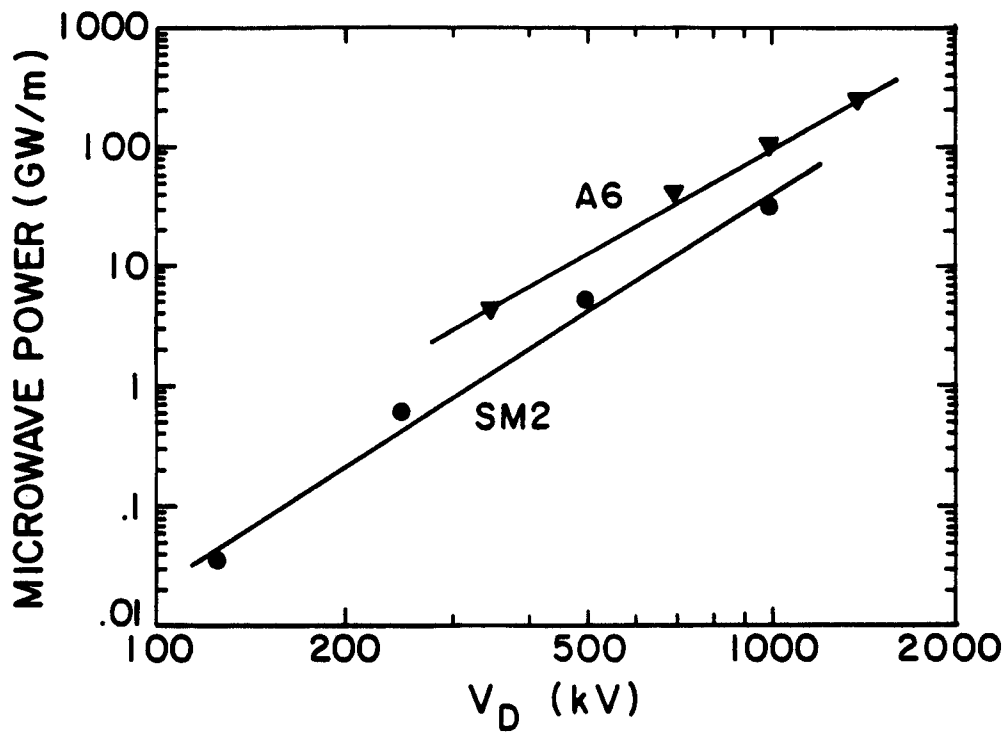


Fig. 7

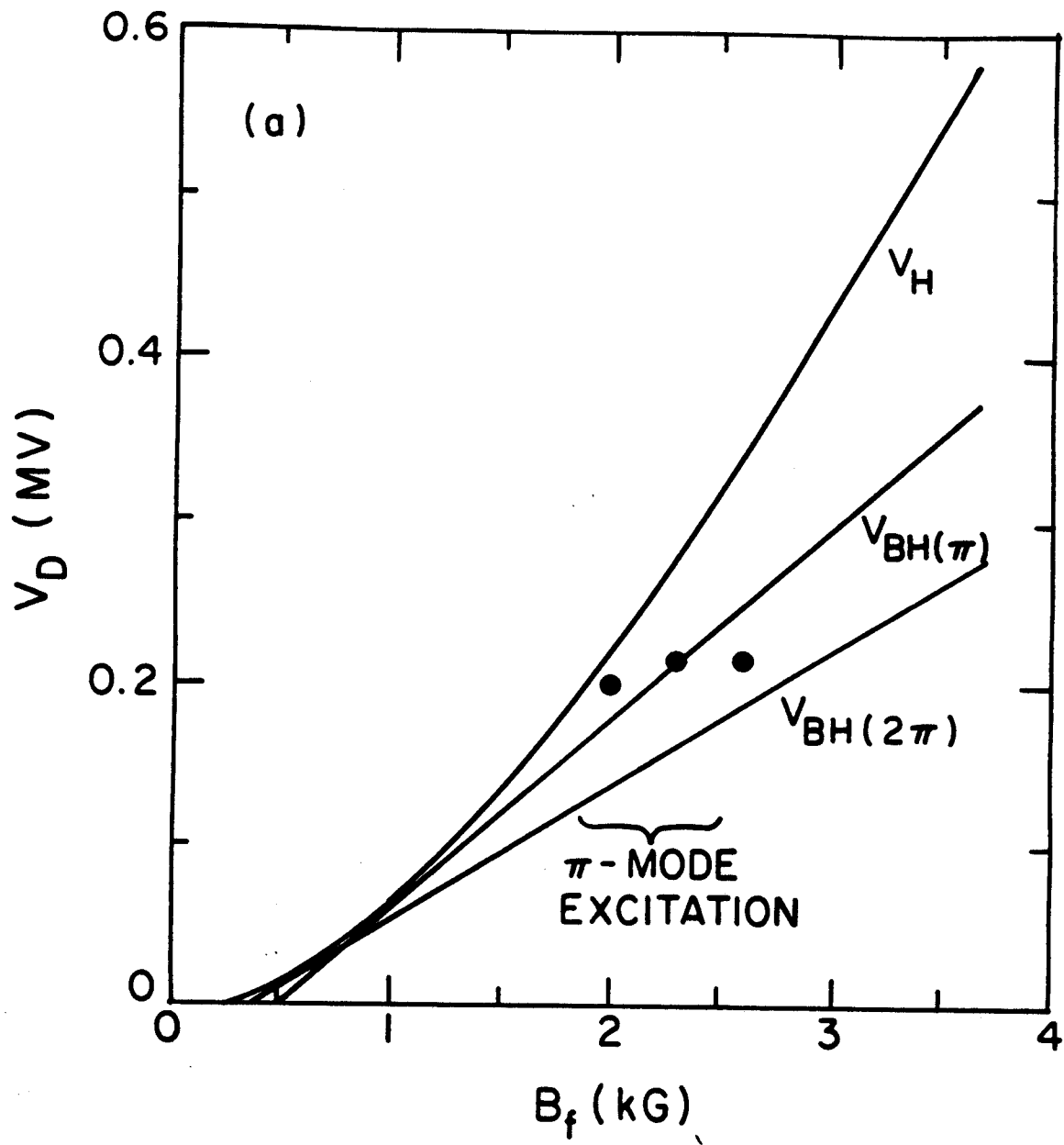


Fig. 8(a)

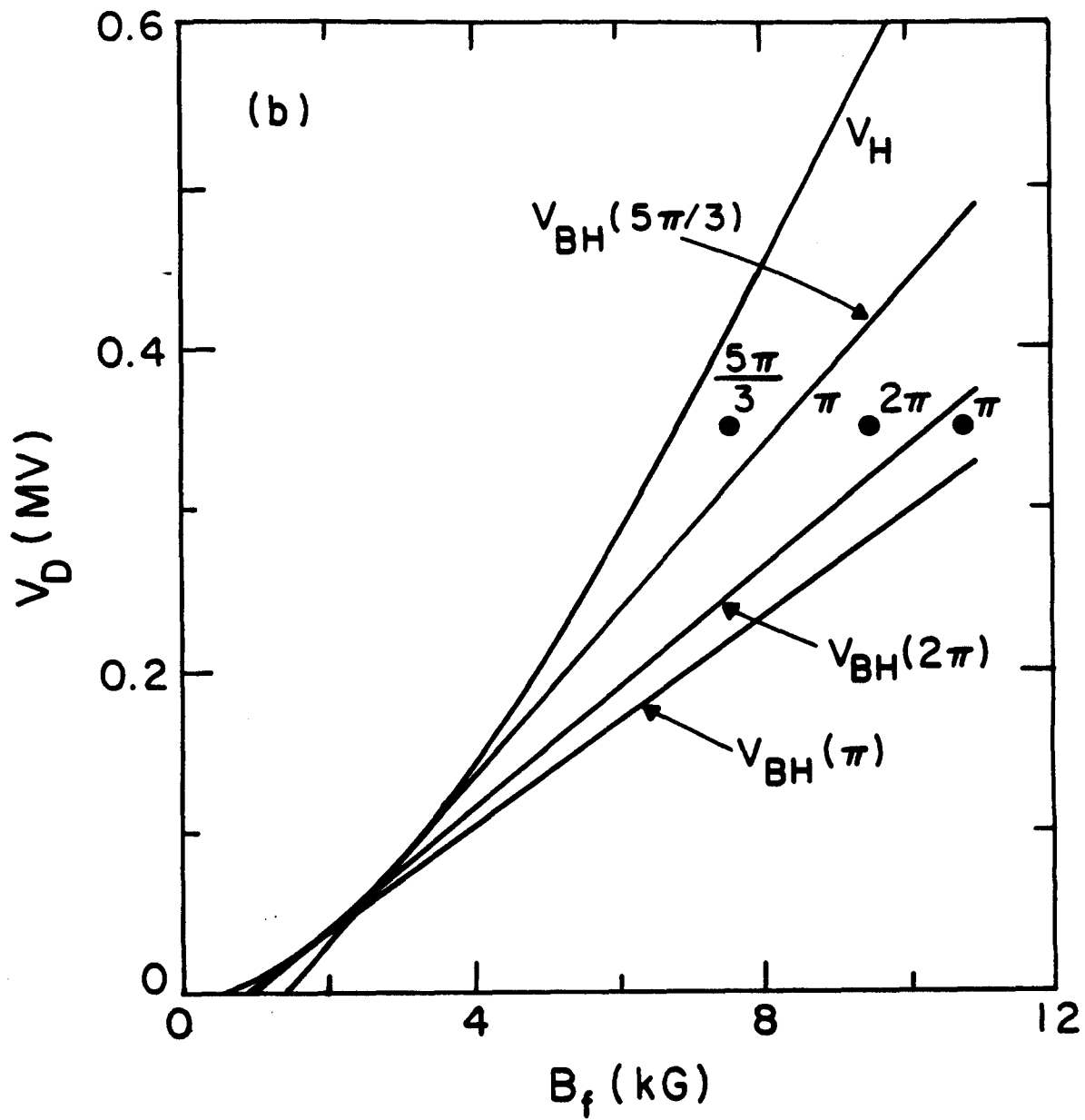


Fig. 8(b)

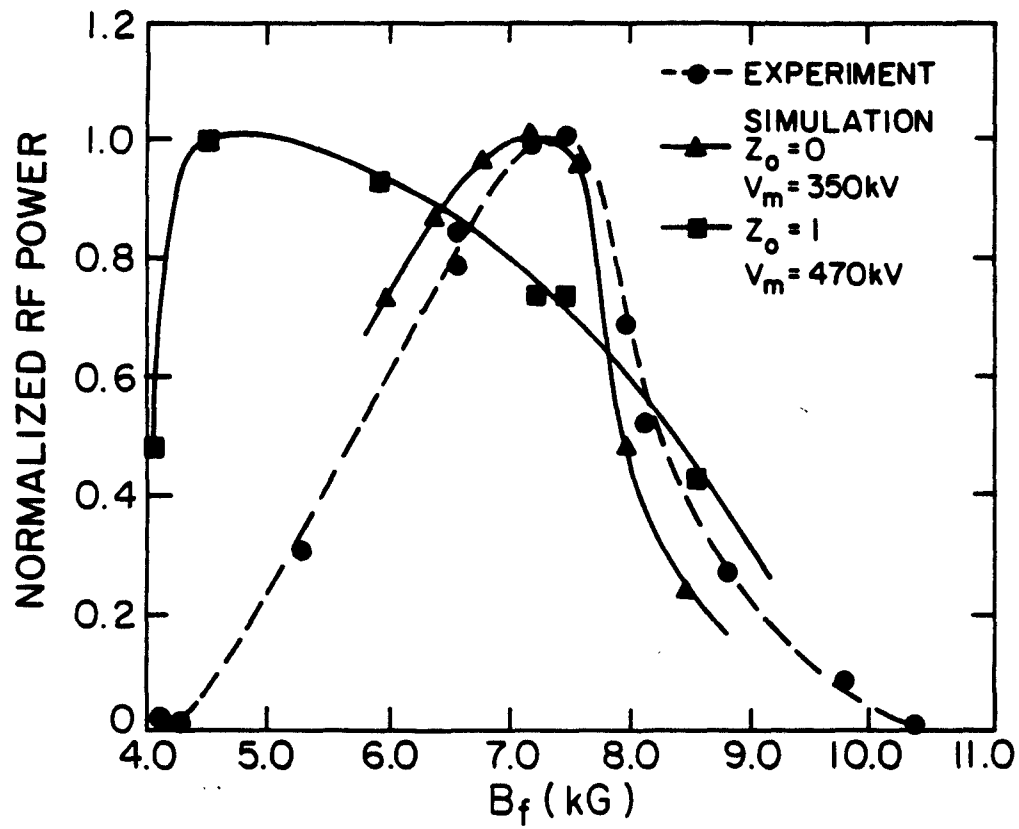


Fig. 9

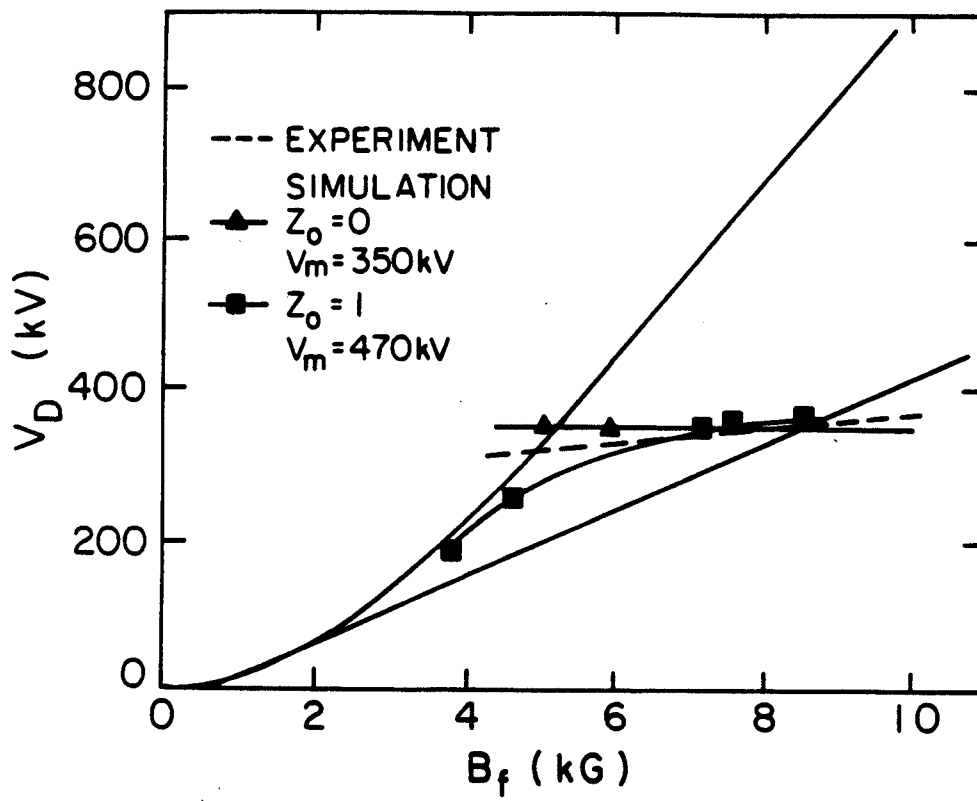


Fig. 10